THE JOURNAL OF BIOLOGICAL CHEMISTRY VOL. 289, NO. 35, pp. 24215–24225, August 29, 2014
© 2014 by The American Society for Biochemistry and Molecular Biology, Inc. Published in the U.S.A.

Constitutive Gα_i Coupling Activity of Very Large G Protein-coupled Receptor 1 (VLGR1) and Its Regulation by PDZD7 Protein*

Received for publication, January 15, 2014, and in revised form, June 19, 2014 Published, JBC Papers in Press, June 24, 2014, DOI 10.1074/jbc.M114.549816

Qiao-Xia Hu[‡1], Jun-Hong Dong[§¶1], Hai-Bo Du[‖1], Dao-Lai Zhang[‡], Hong-Ze Ren[‖], Ming-Liang Ma[‡], Yuan Cai[‡‡], Tong-Chao Zhao[‡], Xiao-Lei Yin[‖], Xiao Yu[§], Tian Xue[‡‡], Zhi-Gang Xu[‖2], and Jin-Peng Sun[‡3]**

*From the [‡]Key Laboratory Experimental Teratology of the Ministry of Education and Department of Biochemistry and Molecular Biology and [§]Department of Physiology, Shandong University School of Medicine, Jinan, Shandong 250012, China, [¶]Weifang Medical University, Weifang, Shandong 261053, China, [‖]Shandong Provincial Key Laboratory of Animal Cells and Developmental Biology, Shandong University School of Life Sciences, Jinan, Shandong 250100, China, **Binzhou Medical University, Yantai, Shandong 264003, China, and [‡‡]School of Life Sciences, University of Science and Technology of China, Hefei, Anhui 230027, China*

Background: The signaling and regulatory mechanism of the orphan receptor VLGR1 remains elusive.
Results: The cleaved VLGR1 β-subunit constitutively coupled to Gα_i and was regulated by the VLGR1 α-subunit, a disease-associated mutation, and PDZD7.
Conclusion: The VLGR1 β-subunit signals independently and is regulated at multiple levels.
Significance: The identified new signaling mechanism may aid in the design of a VLGR1-targeted therapy.

The very large G protein-coupled receptor 1 (VLGR1) is a core component in inner ear hair cell development. Mutations in the *vlgr1* gene cause Usher syndrome, the symptoms of which include congenital hearing loss and progressive retinitis pigmentosa. However, the mechanism of VLGR1-regulated intracellular signaling and its role in Usher syndrome remain elusive. Here, we show that VLGR1 is processed into two fragments after autocleavage at the G protein-coupled receptor proteolytic site. The cleaved VLGR1 β-subunit constitutively inhibited adenylate cyclase (AC) activity through Gα_i coupling. Co-expression of the Gα_{iq} chimera with the VLGR1 β-subunit changed its activity to the phospholipase C/nuclear factor of activated T cells signaling pathway, which demonstrates the Gα_i protein coupling specificity of this subunit. An R6002A mutation in intracellular loop 2 of VLGR1 abolished Gα_i coupling, but the pathogenic VLGR1 Y6236fsx1 mutant showed increased AC inhibition. Furthermore, overexpression of another Usher syndrome protein, PDZD7, decreased the AC inhibition of the VLGR1 β-subunit but showed no effect on the VLGR1 Y6236fsx1 mutant. Taken together, we identified an independent Gα_i signaling pathway of the VLGR1 β-subunit and its regulatory mechanisms that may have a role in the development of Usher syndrome.

Very large G protein-coupled receptor 1 (VLGR1),[4] also called Neurepin, Mass1, or GPR98, is the largest seven-transmembrane receptor and has important functions in hearing and vision systems (1, 2). Mutations of the *vlgr1* gene lead to the development of Usher syndrome, which causes congenital hearing loss and progressive retinitis pigmentosa (3). In addition to sensory dysfunction, the mutation of *vlgr1* is associated with febrile and afebrile seizures (4).

The specific localizations of VLGR1 in the hearing and vision systems agree well with its functional significance. VLGR1 is found in the stereocilia of cochlear hair cells, forming the so-called ankle links (5, 6). In *vlgr1* knock-out mice, the ankle links are missing, the stereocilia are disorganized, and the mice are profoundly deaf (5, 6). In the retina, VLGR1 is expressed at the periciliary membrane complex of photoreceptor cells that is involved in photoreceptor protein trafficking through the connecting cilium (7, 8). Although there is a consensus that VLGR1 plays important roles in the hearing and vision systems, the details of VLGR1-regulated cell signaling and its function as a GPCR remain elusive.

As a seven-transmembrane receptor, VLGR1 belongs to the adhesion GPCR subfamily (or the LNB7TM subfamily) (9). VLGR1 has a very long extracellular region, which includes a pentraxin domain and an epilepsy-associated repeat domain surrounded by 35 calx-β motifs. The C terminus of VLGR1 has seven transmembrane helices and an intracellular C-terminal tail, which contains a PDZ domain-binding interface important for interacting with several Usher proteins, such as Whirlin,

* This work was supported by grants from the National Key Basic Research Program of China Grants 2013CB967700 (to X. Y., T. X., and Z.-G. X.), 2011CB504505 (to Z.-G. X.), and 2012CB910402 (to J.-P. S.); National Natural Science Foundation of China Grants 31371355 (to Z.-G. X.) and 31271505 (to J.-P. S.); Interdiscipline Fund of Shandong University Grants 2012JC021 (to Z.-G. X.) and 2014JC029 (to X. Y.); Independence Innovation Foundation of Shandong University Grant 2012TS114 (to J.-P. S.); and Program for Changjiang Scholars and Innovative Research Team in University Grant IRT13028.
[1] These authors contributed equally to this work.
[2] To whom correspondence may be addressed. E-mail: xuzg@sdu.edu.cn.
[3] To whom correspondence may be addressed. E-mail: sunjinpeng@sdu.edu.cn.

[4] The abbreviations used are: VLGR1, very large G protein-coupled receptor 1; AC, adenylate cyclase; PLC, phospholipase C; NFAT, nuclear factor of activated T cells; GPCR, G protein-coupled receptor; GAIN, GPCR autoproteolysis-inducing; GPS, GPCR proteolytic site; PTX, pertussis toxin; IP_3, inositol 1,4,5-trisphosphate; aa, amino acids; V_{gain}, VLGR1 C-terminal truncation containing transmembrane domain and GAIN domain; V_β, VLGR1 β-subunit; V_n, cleaved V_{gain} N terminus; P, postnatal day; CREB, cAMP-responsive element-binding protein; V_{gs}, V_{gain}-Gα_s; V_{gi}, V_{gain}-Gα_i.

Harmonin, and PDZD7 (10–12). The N-terminal extracellular region of VLGR1 and its seven transmembrane regions are connected by a "GPCR autoproteolysis-inducing (GAIN) domain," which harbors a GPCR proteolytic site (GPS). In many adhesion GPCRs, the GPS undergoes autoproteolysis that separates the receptor into two subunits. Recently, several studies have demonstrated that the cleaved β-subunits (containing the seven-transmembrane region and the C-terminal tail) of these GPCRs independently signals by coupling to specific G protein subtypes (9, 13).

Until now, VLGR1 was regarded as an orphan receptor. However, adenylate cyclase 6 (AC6), a downstream effector of the Gα$_s$ and Gα$_i$ proteins, has been shown to localize at the base of hair cell stereocilia, and this localization is altered in *vlgr1* knock-out mice, suggesting a potential functional coupling between VLGR1 and intracellular cyclase activities (6). Therefore we set out to delineate the specific G protein signaling downstream of VLGR1.

Concurrent with our study, a parallel work showed that a selective combination of various extracellular domains, transmembrane regions, and the C-terminal tail of VLGR1 resulted in extracellular calcium sensation and the activation of Gα$_s$ and Gα$_q$ subtypes as well as increased intracellular cAMP levels and PKC phosphorylation (14). Here, we report that VLGR1 mediates GPCR signaling through another mechanism. VLGR1 undergoes autocleavage at the GPS, which separates the receptor into α- and β-subunits. The cleaved VLGR1 β-subunit activates Gα$_i$ and blocks forskolin-induced cAMP elevation. Specific mutations in VLGR1 intracellular loops, pertussis toxin (PTX) interference, receptor-G protein fusions, and Gα$_{iq}$ chimera experiments further confirmed the specific coupling of Gα$_i$ to the VLGR1 β-subunit. The overexpression of another Usher protein, PDZD7, but not Whirlin or Harmonin, inhibited the VLGR1-Gα$_i$ signaling pathway. In contrast, the Usher syndrome-associated mutant VLGR1 Y6236fsX1 showed enhanced constitutive Gα$_i$ activity, and this activity was not inhibited by PDZD7 most likely due to its lack of a PDZ binding site. Our results indicated that an independent Gα$_i$ signaling pathway is mediated by VLGR1 β-subunit and may further our understanding of the mechanisms underlying Usher syndrome.

EXPERIMENTAL PROCEDURES

Materials—The monoclonal anti-FLAG antibody (F3165), hydroxylamine (NH_2OH) (438227), isoproterenol (I2760), and angiotensin (A2580) were purchased from Sigma. The polyclonal VLGR1 C terminus antibody (sc-21252), polyclonal anti-Myc antibody (sc-789), monoclonal anti-GFP (B2, sc-9996), and monoclonal anti-actin (sc-8432) antibodies were from Santa Cruz Biotechnology. The phospho-CREB-Ser^{133} (9198s) antibody was from Cell Signaling Technology. The GloSensor™ cAMP Assay (E1290) and Dual-Luciferase Reporter Assay System (E1960) were from Promega. Pertussis toxin (*Bordetella pertussis*, BML-G100-0050) was from Enzo Life Sciences. Cell culture medium (3097) was from BD Biosciences. Forskolin (S1612) was from Beyotime. The cAMP ELISA kit (KGE002) was from R&D Systems. The IP_3 ELISA kit was from EIAab® (E2037 Ge). All other chemical and reagents were obtained from Sigma unless otherwise specified.

Constructs—Wild type *vlgr1* C-terminal truncation (V_{gain}) (aa 5618–6298), β-subunit (V_β) (aa 5884–6298), and cleaved V_{gain} N terminus (V_n) (aa 5618–5883) were cloned from mouse inner ear cDNA libraries using the following primers: forward, GATGATGACAAAGCCCTCGAGATGGACATCCTTGATGACAACCTTC and reverse, GTAGAAAAACTGCTGAATTCTCAGAGGTGGGTGTCAGC for V_{gain} or GATGATGACAAAGCCCTCGAGTCTGTGTATGCTGTCTAC for V_β; and forward, CCGCTCGAGGAGCAGAAACTCATCTCTGAAGAGGATCTGGCTGTCTGGGGGCTTGAAG and reverse, CCGCTCGAGGAGCAGAAACTCATCTCTGAAGAGGATCTGTCTAGAGCTGTCTGGGGGCTTGAAG for V_n. The sequences were inserted into the mammalian pcDNA3.1 or pEGFP expression vector. The receptor-effector fusion protein V_{gain}-Gα$_{i2}$ or V_{gain}-Gα$_s$ was constructed with an overlapping PCR method using V_{gain} and G protein cDNAs with the following primers: V_{gain}-Gα$_{i2}$-reverse, CTCACGGTGCAGCCCATGAGGTGGGTGTCAGC; Gα$_{i2}$-forward, GCTGACACCCACCTCATGGGCTGCACCGTGAG; Gα$_{i2}$-reverse, GTAGAAAAACTGCTGAATTCTCAGAAGAGGCCACAGTC; V_{gain}-Gα$_s$-reverse, CCCGAGGCAGCCCATGAGGTGGGTGTCAGC; Gα$_s$-forward, GCTGACACCCACCTCATGGGCTGCCTCGGG; and Gα$_s$-reverse, GTAGAAAAACTGCTGAATTCTTAGAGCAGCTCGTAC. The site-directed VLGR1 and Gα$_i$ mutants, including the Gα$_{i1q}$, Gα$_{i2q}$, Gα$_{i3q}$, V_{gain}-H5882A, V_{gain}-S5884A V_{gain}-F5988A, V_{gain}-Y5990A, and V_{gain}-R6002A mutants, were generated by the QuikChange mutagenesis kit (Stratagene). Plasmids with V_{gain}-Y6236fsx1 (forward, GATGATGACAAAGCCCTCGAGATGGACATCCTTGATGACAACCTTC and reverse, CCGTCGACTGCAGAATTCCTAACCTCCAGAAGAAGG) and V_β-Y6236fsx1 (forward, GATGATGACAAAGCCCTCGAGTCTGTGTATGCTGTCTAC and reverse, CCGTCGACTGCAGAATTCCTAACCTCCAGAAGAAGG) were subcloned by overlapping PCR. The pcDNA3.0-A1TaR, pcDNA3-FLAG-β_2-adrenergic receptor, and dopamine D2 receptor were generous gifts from Professor Robert J. Lefkowitz at Duke University. All constructs were subjected to DNA sequencing to verify sequence identities.

Animals and Cochlea Isolation—All animal care and experiments were reviewed and approved by the Animal Use Committee of the Shandong University School of Medicine. *Gpr98^{tm1Pwh}*/J mice were purchased from The Jackson Laboratory (Bar Harbor, ME) and maintained in pathogen-free conditions at Shandong University. For cochlear protein preparation, P21 C57BL/6 and *Gpr98^{tm1Pwh}*/J mice were euthanized by rapid decapitation, the cochlea were quickly removed, and the proteins were prepared with lysis buffer as described previously (15).

Cell Culture, Transfection, and Western Blotting—Human embryonic kidney 293 (HEK293) cells, U251 cells, and GloSensor HEK293 cells were maintained in Dulbecco's modified Eagle's medium or modified Eagle's medium, respectively, supplemented with 10% heat-inactivated fetal bovine serum (Hyclone Thermo Scientific, Scoresby, Victoria, Australia). PC12 cells were maintained in Dulbecco's modified Eagle's medium with 5% heat-inactivated fetal bovine serum and 5% donor equine serum (Hyclone Thermo Scientific, SH30074.03). For receptor or other protein expression, plasmids carrying

the desired genes were transfected into cells using Lipofectamine™ 2000 (Invitrogen). To monitor protein expression levels, cells were collected 48–72 h post-transfection with lysis buffer (50 mM Tris, pH 8.0, 150 mM NaCl, 1 mM NaF, 1% Nonidet P-40, 2 mM EDTA, 10% glycerol, 0.25% sodium deoxycholate, 1 mM Na_3VO_4, 0.3 μM aprotinin, 130 μM Bestatin, 1 μM leupeptin, 1 μM Pepstatin, and 0.5% iodoamino acids). Cell lysates were subjected to end-to-end rotation for 20 min and spun at 12,000 rpm for 20 min at 4 °C. Then an equal volume of 2× loading buffer was added. Proteins were denatured in loading buffer and subjected to Western blot analysis. The protein bands from Western blots were quantified with ImageJ software (National Institutes of Health, Bethesda, MD).

Retina Preparation and in Vivo Transfection—Before transfection, the plasmids were prepared as follows. The *vgr1* (aa 5618–6298)-GFP or pcDNA3.1 control plasmid was mixed with 0.1 volume of 3 M sodium acetate and 2.5 volumes anhydrous ethanol. The mixture was bathed in ice for 15 min, centrifuged at 14,000 × *g* at 4 °C, and then washed and precipitated with anhydrous ethanol. The plasmids were further dried, resuspended in PBS, and adjusted to a concentration of 5 μg/μl.

For transfection, newborn (P0–P3) mouse pups (C57BL/6) were anesthetized on ice for 5 min. The eyes were carefully opened by cutting along the closed eyelid using a sharp 26-gauge needle, and then a small incision was made in the sclera. A 20-μm micropipette (P-1000, Sutter Instruments) was inserted into the incision until the tip of micropipette touched the opposing sclera. Then 0.5 μl of high concentration plasmid DNA were slowly injected into the subretina (Nanoject II) followed by electroporation five pulses of 80 volts for 50 ms with 950-ms intervals using a Digidata 1440A pulse generator from Axon CNS Instruments (16). Three days after electroporation, the eyes were dissected, and the retinas were isolated for further experiments.

In Vitro Cleavage of V_{gain} Proteins—HEK293 cells were transfected with a FLAG-V_{gain} or V_{gain}-GFP plasmid in 10-cm plates. Forty-eight hours after transfection, cells were washed three times with ice-cold PBS and incubated with lysis buffer for 45 min with end-to-end rotation. After a 12,000 rpm centrifugation for 30 min, the supernatants were collected. One hundred micrograms of protein were added to 100 μl of cleavage buffer (50 mM Tris, pH 7.5, 20 mM NaCl, and 1 mM EDTA) and incubated at 37 °C for the desired time. Loading buffer was added to samples, and samples were analyzed by Western blotting. For NH_2OH-facilitated receptor hydrolysis, the receptor was immunoprecipitated with anti-FLAG M2 affinity gel as described previously (17). The immunoprecipitated receptors were incubated with 250 mM NH_2OH for the indicated times before examination by Western blotting.

CREB Phosphorylation—HEK293 cells transfected with the desired plasmids were maintained in medium and starved for 8 h. After a 10-min application of 10 μM forskolin or mock solution, the cells were quickly transferred to ice and incubated with cell lysis buffer. The cell lysates were subjected to Western blotting, and CREB phosphorylation levels were detected using a phospho-CREB-Ser^{133} antibody.

IP_3 ELISA—Cells were washed with cold PBS followed by three freeze-thaw cycles in liquid nitrogen. The cells were then lysed for another 20 min at 4 °C with end-to-end rotation. After centrifugation at 12,000 rpm for 15 min at 4 °C, the supernatant was collected to determine IP_3 concentrations according to the manufacturer's instructions (EIAab, E2037 Ge).

GloSensor cAMP Assay—GloSensor 22-F cells were transfected with the desired plasmids (0.8 μg of total DNA) with Lipofectamine 2000 in 24-well dishes. Twenty-four hours later, cells were plated on 96-well plates at a cell density of 20,000 cells/well. Cells were maintained in culture medium for another 22 h and washed with PBS. Cells were then incubated with 100 μl of equilibration medium (2% (v/v) GloSensor cAMP Reagent, 10% FBS, and 88% CO_2-independent medium) in each well for 2 h. The basal cAMP signal was measured using a luminescence counter (Mithras LB 940). After the cAMP levels reached a steady baseline for more than 5 min, 10 μM forskolin was added to determine the effects of forskolin-stimulated cAMP increase. For PTX treatment, 100 ng/ml PTX was preincubated with cells for at least 16 h. Data are presented as the mean ± S.D. Statistical comparisons were performed with analysis of variance tests using GraphPad Prism5.

cAMP ELISA—HEK293 cells transfected with desired plasmids were cultured in 96-well plates. 48 h later, cells were washed three times with PBS and stimulated. After a certain time, cells were resuspended in 120 μl of lysis buffer (1×) with 500 μM isobutylmethylxanthine for each well and then frozen at −20 °C. Cells underwent two freeze-thaw cycles and then were subjected to centrifugation (600 × *g*) for 10 min at 4 °C to remove cellular debris. The supernatant were assessed for cAMP content according to the manufacturer's protocol (cAMP ELISA kit (KGE002) for R&D Systems).

NFAT Dual-Luciferase Reporter Assay—HEK293 cells were transfected using Lipofectamine 2000 in 24-well dishes with 0.8 μg of total DNA, including V_{gain} or V_β, $G\alpha_{i1q}$, $G\alpha_{i2q}$, $G\alpha_{i3q}$, A1TaR, dopamine D2 receptor, pGL3-NFAT luciferase or pGL3-Basic luciferase, and the pRL-TK plasmid (Promega, Madison, WI). Cells were cultured for 48 h and then harvested immediately following addition of 1× passive lysis buffer. After incubation for 15 min at room temperature on a table shaker, cell lysates were centrifuged at 12,000 rpm for 10 min at 4 °C. NFAT activity was quantified by a standard luciferase reporter gene assay and was normalized to *Renilla* luciferase activity (Promega). More than three independent experiments in 8 wells were performed for each *Dual-Luciferase reporter* assay.

Immunofluorescence—FLAG-tagged V_β- or V_β-Y6236fsx1-transfected cells grown on glass coverslips in 24-well tissue culture plates were fixed with 4% paraformaldehyde in phosphate-buffered saline. The cells were blocked and permeabilized with blocking buffer containing 0.1% Triton X-100 and 1% normal goat serum for 60 min at room temperature. Cells were then incubated sequentially with a primary anti-FLAG antibody at 4 °C overnight and an appropriate secondary antibody for 1 h at room temperature. Immunofluorescence was analyzed on a Bio-Rad Radiance 2000 laser-scanning confocal microscope.

Co-immunoprecipitation—Co-immunoprecipitation experiments were performed as described previously (17). Plasmids encoding FLAG-V_{gain}, FLAG-V_β, Myc-V_n, or Myc-PDZD7 and control pcDNA3.1 were transfected or co-transfected into HEK293 cells that were cultured in 150-mm dishes. After

allowing 30 h of protein expression, the cells were washed with phosphate-buffered saline containing 10 mM HEPES, pH 7.5. Cells were lysed in lysis buffer (50 mM Tris, pH 7.4, 150 mM NaCl, 1% Nonidet P-40, 0.5% sodium deoxycholate, 2 mM sodium pyrophosphate, 5 mM NaF, 25 mM β-glycerophosphate, 1 mM EDTA, and 1 mM Na_3VO_4 supplemented with protease inhibitor mixture (Roche Applied Science)). Cell lysates were then incubated with anti-FLAG M2 affinity gel (Sigma-Aldrich) for 4–6 h, and the FLAG-tagged V_{gain} or V_β was precipitated by centrifugation. After extensive bead washing with PBS buffer, the immunoprecipitated complexes were subjected to electrophoresis, and complex formation was detected by Western blotting with an anti-Myc antibody.

Data Analysis—All data are presented as the mean ± S.D. from at least three independent experiments. Statistical comparisons were performed with analysis of variance tests using GraphPad Prism5. Significant differences were designated as follows: * and #, $p < 0.05$; ** and ##, $p < 0.01$; and *** and ###, $p < 0.005$. The sequence alignments were performed using T-Coffee.

RESULTS AND DISCUSSION

VLGR1 Can Be Processed into Two Fragments after Autoproteolysis—VLGR1 contains a GPS immediately preceding its seven-transmembrane domain (1). Many adhesion GPCRs have been shown to undergo self-proteolysis at the GPS and

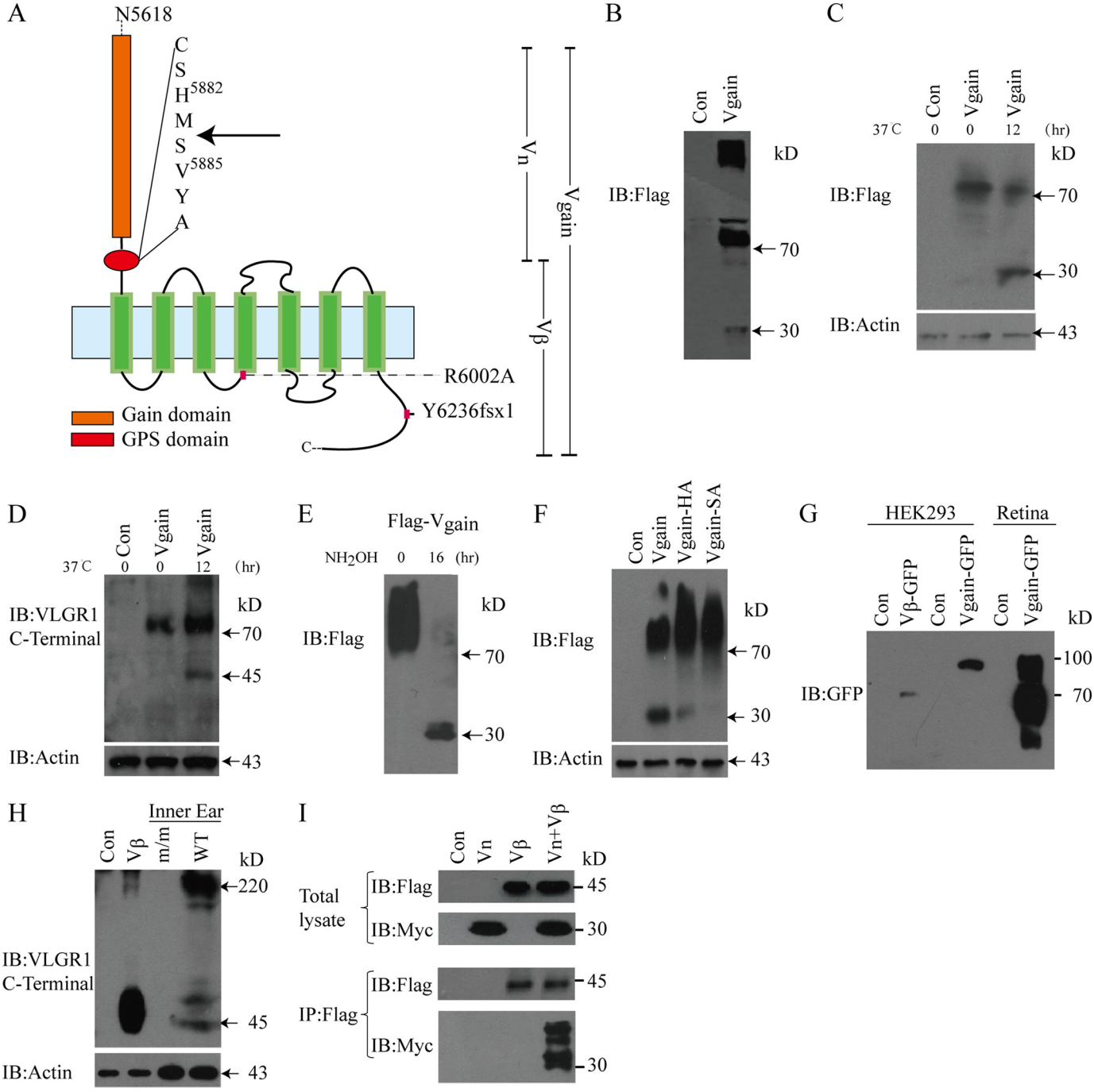

generate two subunits to form a heterodimeric complex (9, 13). Recent crystallographic studies have discovered that the 40-residue GPS motif is located in an intact ~320-residue domain called the GAIN domain. Biochemical studies show that the GAIN domain of several adhesion GPCRs is both necessary and sufficient for autocleavage (18).

The full-length VLGR1 encompasses ~6300 amino acids and thus is difficult to analyze by electrophoresis (1, 14). To test whether VLGR1 can be processed into two fragments in a manner similar to other adhesion GPCRs, we made a construct of the C-terminal portion of VLGR1 (aa 5618–6298; V_{gain}) that contained the intact GAIN domain, the seven-transmembrane region, and the intracellular C-terminal tail (Fig. 1*A*). In cells transfected with the FLAG-V_{gain}-expressing plasmid, a 75-kDa band was detected that is consistent with the size of full-length FLAG-V_{gain}. Several bands with molecular masses higher than 130 kDa were also evident, presumably due to glycosylation or dimerization (Fig. 1*B*). FLAG-V_{gain} was mainly expressed as an intact protein; however, at ~35 kDa, a weak band corresponding to the N-terminal portion of FLAG-V_{gain} after cleavage at GPS was also detected (Fig. 1*B*). We then incubated the cell lysates at 37 °C to promote FLAG-V_{gain} autoproteolysis. The 35-kDa band corresponding to the cleaved N-terminal fragment increased abundantly, whereas the 80-kDa full-length FLAG-V_{gain} band decreased in intensity (Fig. 1*C*). Accordingly, the 45-kDa band corresponding to the cleaved C-terminal fragment of VLGR1 was detected by a specific VLGR1 C terminus antibody after incubation at 37 °C (Fig. 1*D*). Moreover, similar to the chemical cleavage that occurs at the GPS of other adhesion GPCRs, the autocleavage of VLGR1 can also be accelerated by the strong nucleophile NH_2OH (Fig. 1*E*) (19).

To further demonstrate the presence of the autocleavage site, we examined the effects of specific VLGR1 GPS mutations on VLGR1 autoproteolysis. Previous studies have revealed the essential role of the conserved H(L/M)(S/T) motif for autocleavage at the GPS (18, 19). Although His^{516} of EMR2 is the proton acceptor for the generation of the tetrahedral intermediate and deprotonates the hydroxyl group of Ser^{518}, the deprotonated oxygen of Ser^{518} is important for the nucleophilic attack of the C–N ester bond that produces two polypeptide fragments (19). Therefore, we mutated the corresponding conserved His^{5882} and Ser^{5884} residues to Ala and examined their effects on VLGR1 autoproteolysis (Fig. 1*F*). The V_{gain}-H5882A mutant reduced autoproteolysis, and the V_{gain}-S5884A mutant almost abolished autoproteolysis. These results suggested that specific autoproteolysis occurred at the GPS.

Endogenous VLGR1 has been detected in many tissues, including brain, lung, kidney, eye, and cochlea (1, 3, 5, 20–22). In humans, mutations in VLGR1 cause type IIC Usher syndrome, which results in congenital hearing loss and progressive retinitis pigmentosa (1, 23). These genetic studies implied that the VLGR1 has important functions in the inner ear and retina. Therefore, we chose both the retina and cochlea as physiological models to investigate VLGR1 autocleavage along with the HEK293 cell system (Fig. 1, *G* and *H*). We transfected pcDNA3.1 control plasmids or V_{gain} (aa 5618–6298)-GFP plasmids into the retina of the newborn (P0–P3) mouse pups (C57BL/6). After 3 days of protein expression postelectroporation, mouse pup eyes were dissected, and the expression of V_{gain} was detected with a GFP antibody. Similar to the FLAG-V_{gain}-transfected HEK293 cells, a single band corresponding to the intact V_{gain}-GFP size (100 kDa) was mainly detected in the V_{gain}-transfected HEK293 cells (Fig. 1, *B* and *G*). However, a cleaved band corresponding to the V_{β}-GFP (68 kDa) was detected in V_{gain}-transfected retina, suggesting that autocleavage was more likely to happen in a more physiological context (Fig. 1*G*). Next, we used inner ear tissue from $Gpr98^{tm1Pwh}$/J mice or their C57BL/6 wild type littermates to examine endogenous VLGR1 expression. The $Gpr98^{tm1Pwh}$/J mouse has a deletion of its seven-transmembrane and cytoplasmic regions. As shown in Fig. 1*H* in wild type cochlea, a 220-kDa band corresponding to VLGR1a (the shortest VLGR1 isoform) and a 45-kDa band corresponding to the VLGR1 β-subunit were detected by a specific VLGR1 C terminus antibody, whereas these bands were not detected in $Gpr98^{tm1Pwh}$/J mice.

FIGURE 1. **V_{gain} underwent autoproteolysis that generated V_{β}.** *A*, a schematic diagram of the structure of the VLGR1 constructs used in the study. V_{gain}, aa 5618–6298 of VLGR1, includes the GAIN domain, the seven-transmembrane region, and the intracellular C-terminal tail. V_{β}, aa 5884–6298 of VLGR1, corresponds to the region from the GPS cleavage site to the C terminus and includes the seven-transmembrane region and the intracellular C-terminal tail. V_n, aa 5618–5883 of VLGR1, is the N-terminal region of the GAIN domain. The residues of the GPS are displayed, and the autoproteolytic position is indicated by an *arrow*. The disease-related VLGR1 mutations, Y6236fsx1 in the C terminus and R6002A in the second intracellular loop, both of which were used in this study, are highlighted. *B*, Western blot of V_{gain} truncation (aa 5618–6298). Cells were transiently transfected with N-terminal FLAG-tagged V_{gain} and control pcDNA3.1 plasmids. The expression of V_{gain} was detected by anti-FLAG antibody. The *top arrow* indicates the expression of FLAG-V_{gain} with a calculated molecular mass of 74 kDa. The *lower arrow* indicates a 35-kDa band that corresponded to the molecular mass of the cleaved N-terminal V_{gain} fragment. Several bands with molecular masses greater than 130 kDa were also detected. *C* and *D*, VLGR1 undergoes autoproteolysis in HEK293 cells. HEK293 cells were transiently transfected with plasmids to express N-terminal FLAG-tagged V_{gain} or control pcDNA3.1 plasmid. The cell lysates were incubated at 37 °C for 0 or 12 h. The cleaved and uncleaved fragments were examined using an anti-FLAG antibody (*C*) or a specific VLGR1 C terminus antibody (*D*). *E*, NH_2OH-facilitated cleavage of V_{gain} at GPS. Cells were transfected with V_{gain} plasmids. After 48 h, cells were collected, and the cell lysates were incubated at 37 °C with or without 250 mM NH_2OH in cleavage buffer. After 16 h, most of the 74-kDa V_{gain} bands were cleaved, generating the 30-kDa band corresponding to the N-terminal fragment of the V_{gain} truncation. *F*, effects of GPS mutations on NH_2OH-facilitated V_{gain} cleavage. HEK293 cells were transiently transfected with plasmids containing the FLAG-tagged wild type V_{gain}, V_{gain}-H5882A (*HA*) mutant, V_{gain}-S5884A (*SA*) mutant, or control pcDNA3.1. FLAG-tagged V_{gain} was immunoprecipitated and incubated with 250 mM NH_2OH to facilitate cleavage. The cleaved receptor was detected with an anti-FLAG antibody. *G*, VLGR1 underwent autoproteolysis and produced the truncated V_{β} in mouse retina. Mouse retina was transiently transfected with the control pcDNA3.1 plasmid or a plasmid encoding a C-terminal GFP-tagged V_{gain}. Three days were allowed for protein expression, and VLGR1 expression was detected with a GFP antibody. The transient expressions of V_{β}-GFP (aa 5884–6298) and V_{gain}-GFP (aa 5618–6298) in HEK293 cells were used as controls. Multiple bands were detected in GFP-tagged V_{gain}-infected mouse retina, including the 80-kDa GFP-tagged fragment, which corresponded to the cleaved V_{β}-GFP. *H*, detection of endogenous VLGR1 in mouse cochlea. VLGR1 expression in the inner ear at P21 of the VLGR1 mutant mice (lacking the seven-transmembrane domain and cytoplasmic tail) (*m/m*) and the wild type (WT) mice were detected with a specific VLGR1 C terminus antibody. The transiently expressed FLAG-V_{β} in HEK293 cells was used as a control. A band around the same size as FLAG-V_{β} was detected with the VLGR1 C terminus antibody in WT mice but not in VLGR1 mutant mice. *I*, direct interaction between V_{β} and V_n (aa 5618–5883). FLAG-tagged V_{β} was co-transfected with Myc-tagged V_n or control pcDNA4 plasmid. The V_{β} and its associated proteins were immunoprecipitated with an anti-FLAG antibody, and the formation of the V_{β}·V_n complex was detected with anti-Myc antibody. *Con*, control; *IB*, immunoblot.

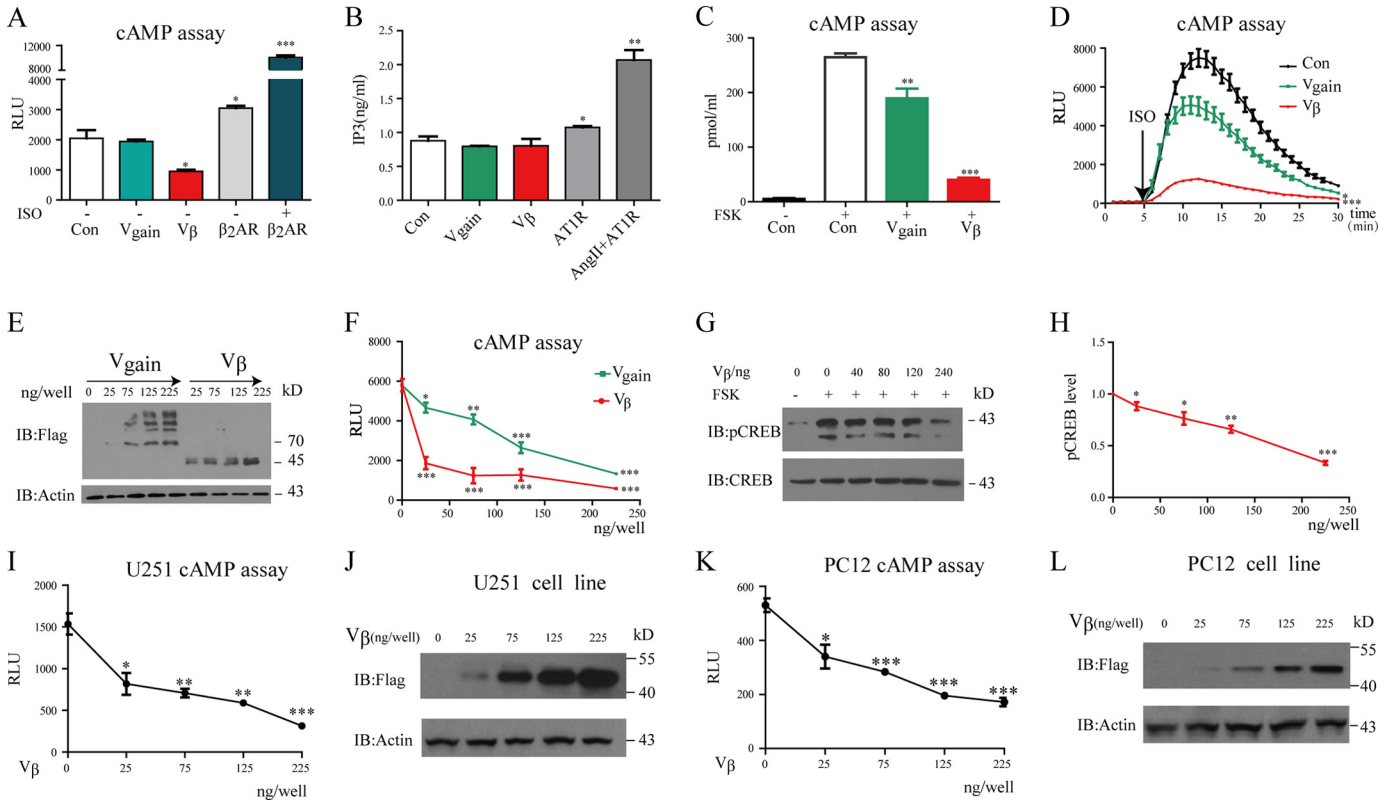

FIGURE 2. **V_{gain} and the cleaved V_β inhibited forskolin- and isoproterenol-induced cAMP elevation.** *A*, effects of overexpression of V_{gain} or V_β on basal cAMP level. HEK293 GloSensor cells were transfected with V_{gain}, V_β, or β_2-adrenergic receptor (β_2AR) plasmids. After 46 h, the basal cAMP levels were monitored by the GloSensor assay. The β_2-adrenergic receptor-transfected cells were used as a positive control. Overexpression of the β_2-adrenergic receptor increased the basal cAMP level. The cAMP level can be further augmented by treating the β_2-adrenergic receptor-transfected cells with its agonist, isoproterenol. In contrast, there is no basal cAMP level increase for V_{gain}-transfected cells. Overexpression of V_β decreases, rather than increases, the basal cAMP level. One-way analysis of variance was used for statistical analysis. *, $p < 0.05$; **, $p < 0.01$; ***, $p < 0.005$. *Error bars* represent S.D. *B*, effects of overexpression of V_{gain} or V_β on IP_3 generation. HEK293 cells were transfected with V_{gain}, V_β, or A1TaR plasmids. After 46 h, the basal IP_3 levels were monitored with an ELISA kit. The A1TaR-transfected cells were used as a positive control. Overexpression of A1TaR increased basal IP_3 levels. The IP_3 levels were further stimulated by treating the cells with angiotensin II. An increase in IP_3 levels was not detected in V_{gain}- or V_β-transfected cells. One-way analysis of variance was used for statistical analysis. *, $p < 0.05$; **, $p < 0.01$. *Error bars* represent S.D. *C*, the overexpression of V_{gain} or V_β blocked the forskolin-induced cAMP increase. HEK293 cells were transfected with the control pcDNA vector or the V_{gain} or V_β expression vector. The absolute cAMP levels were measured using an ELISA kit. *Error bars* represent S.D. *D*, the overexpression of V_{gain} or V_β blocked the isoproterenol-induced cAMP increase. GloSensor cAMP HEK293 cells were transiently transfected with the control pcDNA vector or the V_{gain} or V_β expression vector. The kinetic responses of the cells to isoproterenol were monitored with FLIPR^{TETRA}. *Error bars* represent S.D. *E* and *F*, the dose-dependent inhibition of the forskolin-induced cAMP increase by overexpression of V_{gain} or V_β. GloSensor HEK293 cells were transfected with the control pcDNA vector or the V_{gain} or V_β expression vector at the indicated concentrations. The protein expression levels were examined using a FLAG-specific antibody (*E*). The forskolin-induced cAMP increase was examined using FLIPR^{TETRA} (*F*). *Error bars* represent S.D. *G*, the effect of dose-dependent inhibition of V_β on forskolin-induced CREB phosphorylation. HEK293 cells were transfected with control plasmids or the indicated amounts of the V_β plasmids. The phosphorylation of CREB at Ser^{133} was examined using a specific antibody following forskolin stimulation. *H*, statistics of *G*. *, $p < 0.05$; **, $p < 0.01$; ***, $p < 0.005$ for V_β-transfected cells compared with non-V_β-transfected cells. *Error bars* represent S.D. *I–L*, the dose-dependent inhibition of the forskolin-induced cAMP increase by overexpression of V_β in U251 astrocyte cells (*I* and *J*) or PC12 cells (*K* and *L*). GloSensor plasmids were co-transfected with the control pcDNA vector or the V_{gain} or V_β expression vector at the indicated concentrations in U251 cells (*I* and *J*) or PC12 cells (*K* and *L*). The protein expression levels were examined using a FLAG-specific antibody (*J* and *L*). The forskolin-induced cAMP increase was examined using FLIPR^{TETRA} (*I* and *K*). *, $p < 0.05$; **, $p < 0.01$; ***, $p < 0.005$ for V_β-transfected cells compared with non-V_β-transfected cells. *Error bars* represent S.E. *ISO*, isoproterenol; *FSK*, forskolin; *Con*, control; *IB*, immunoblot; *RLU*, relative luciferase units; *β2AR*, β_2-adrenergic receptor; *AngII*, angiotensin II; *pCREB*, phospho-CREB.

Several studies have also suggested that the two cleaved subunits of the adhesion GPCRs still maintain a complex via non-covalent interactions (13, 18). Therefore, we overexpressed the FLAG-tagged V_β and the Myc-tagged V_n (aa 5618–5883) in HEK293 cells. As shown in Fig. 1*I*, the complex formation of the two fragments of V_{gain} was detected by co-immunoprecipitation assays.

V_{gain} and V_β Constitutively Inhibit the AC Pathway—Most of the two cleaved subunits (α-subunit corresponds to the N-terminal segment, and β-subunit corresponds to the C-terminal segment) of adhesion GPCRs still bind to each other to form heterodimers. In several cases, the β-subunit signals independently of the α-subunit, whereas the α-subunit serves as an inhibitor for the constitutive activity of the β-subunit (9, 13, 24). Without a known ligand, overexpression of an adhesion GPCR or its β-subunit constitutively activates specific signaling pathways that are normally stimulated by agonist activation (13, 24, 25). The constitutive activities of orphan receptors have been used to characterize their downstream signaling activities (26, 27).

Therefore, we made V_β (aa 5884–6298) and examined the ability of the receptor to constitutively activate the classic G protein signaling pathways. The overexpression of V_{gain} or V_β did not increase the basal intracellular cAMP levels or IP_3 accumulation, indicating that $G\alpha_s$ and $G\alpha_q$, respectively, are not constitutively activated by V_{gain} and V_β (Fig. 2, *A* and *B*). In contrast, the overexpression of V_{gain} or V_β significantly blocked the forskolin-induced intracellular cAMP increase, suggesting

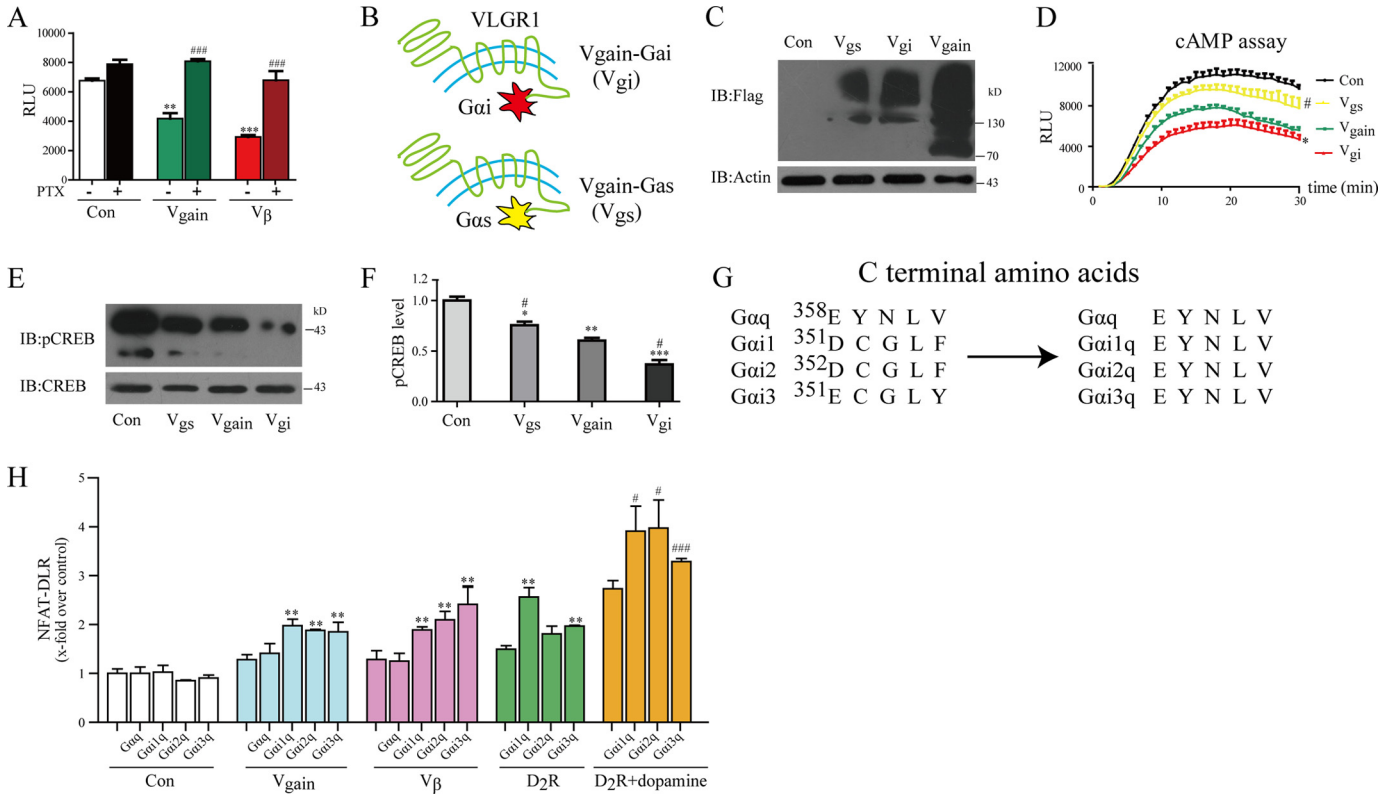

FIGURE 3. **V_{gain} and V_β inhibited intracellular cAMP formation by Gα_i coupling.** *A*, PTX blocked the V_{gain}- or V_β-mediated cAMP inhibition. GloSensor cAMP HEK293 cells were transfected with either empty vector (*Con*), V_{gain}, or V_β and then treated with 100 ng/ml PTX for 6 h followed by stimulation with forskolin. The intracellular cAMP levels were monitored using FLIPR^{TETRA}. ***, $p < 0.005$ compared with control; ###, $p < 0.005$ compared with non-PTX treated cells. *Error bars* represent S.D. *B*, a schematic representation of the V_{gi} and V_{gs} fusion proteins. The start codon of Gα_{i2} or Gα_s was placed immediately after the 3′-end of the coding region for VLGR1. *C*, the expression of N-terminal FLAG-tagged V_{gs}, V_{gi}, and V_{gain} were examined using a FLAG-specific antibody. *D*, covalently linking V_{gain} to Gα_i leads to an enhanced constitutive activity, whereas linking V_{gain} to Gα_s blocks its constitutive activity. GloSensor cAMP HEK293 cells were transfected with either empty vector, V_{gain}, V_{gi}, or V_{gs}. The forskolin-induced cAMP increase was monitored with FLIPR^{TETRA}. *Error bars* represent S.D. *E*, effects of overexpression of V_{gain}, V_{gi}, or V_{gs} on the forskolin-induced CREB phosphorylation. CREB phosphorylation was examined using a phospho-CREB-Ser^{133}-specific antibody. *F*, statistics of *E*. *, $p < 0.05$; **, $p < 0.01$; ***$p < 0.005$ for V_{gain}-, V_{gi}-, or V_{gs}-transfected cells compared with control vector-transfected cells; #, $p < 0.05$ for V_{gi}- or V_{gs}-transfected cells compared with V_{gain}-transfected cells. *Error bars* represent S.D. *G*, the methodology for the generation of the Gα_{iq} chimeric proteins. The last five C-terminal residues of the corresponding Gα_i proteins were replaced with the last five C-terminal residues of the Gα_q protein that are important for the stimulation of PLC activity. *H*, the plasmids encoding the Gα_q or the Gα_{iq} chimeric proteins were co-transfected with the control vector, V_{gain}, or V_β. The activation of the Gα_{iq}-PLC pathway was assayed by detecting the luciferase activity of the NFAT-driven luciferase reporter gene. The known Gα_i-coupled receptor D2 receptor was used as a positive control. *Error bars* represent S.D. *RLU*, relative luciferase units; *Con*, control; *IB*, immunoblot; *pCREB*, phospho-CREB; *D_2R*, dopamine D2 receptor.

a negative regulatory role for V_{gain} and V_β (Fig. 2*C*). To confirm these results, we used isoproterenol to stimulate endogenous β_2-adrenergic receptor in HEK293 cells and kinetically monitored the effects of V_{gain} or V_β on the isoproterenol-stimulated AC activity using the GloSensor assay. Again, the expression of V_{gain} or V_β significantly suppressed the isoproterenol-induced increase in intracellular cAMP (Fig. 2*D*). Compared with V_{gain}, V_β displayed an enhanced constitutive activity in the inhibition of the intracellular cAMP level in both experiments.

The constitutive activity of a GPCR is often in proportion to its expression level (26). To test whether this is also the case for VLGR1, we overexpressed various amounts of V_{gain} or V_β in HEK293 GloSensor cells. In agreement with our hypothesis, increased expression of either V_{gain} or V_β showed more inhibitory activity toward forskolin-induced cAMP elevation (Fig. 2, *E* and *F*). Consistently, the overexpression of V_β down-regulated the forskolin-induced phosphorylation of CREB at amino acid 133, the downstream target of AC activation, in a dose-dependent manner (Fig. 2, *G* and *H*). To examine the V_β-mediated signaling in a more physiological context, we overexpressed the V_β in neuronal glioblastoma (astrocytoma) cell line U251 and the neuronal PC12 cell line and checked their effects on the forskolin-induced cAMP increase (Fig. 2, *I–L*). Similar to the results in the HEK293 cells, the constitutive AC inhibitory activity of V_β is in proportion to its expression level in both U251 (Fig. 2, *I* and *J*) and PC12 cells (Fig. 2, *K* and *L*). Taken together, these results show that V_{gain} and the VLGR1 β-subunit constitutively inhibit the AC pathway and that V_β has a stronger effect than V_{gain}.

G Protein Coupling Specificity of V_{gain} and the VLGR1 β-Subunit—We then examined whether the constitutive activity of V_{gain} and the VLGR1 β-subunit toward the regulation of intracellular cAMP levels is mediated via Gα_i using its inhibitory protein, PTX. Incubation of the cells with PTX abolished the inhibition of V_{gain} and V_β on AC activity, suggesting that V_{gain} and V_β are indeed coupled to Gα_i (Fig. 3*A*). To further dissect the G protein coupling specificity of V_{gain} and V_β, we next examined the effects of V_{gain}-Gα_s (V_{gs}) and V_{gain}-Gα_i (V_{gi}) fusion proteins (Fig. 3, *B* and *C*). It has been shown that putting the receptor and effector together by receptor-effector fusion

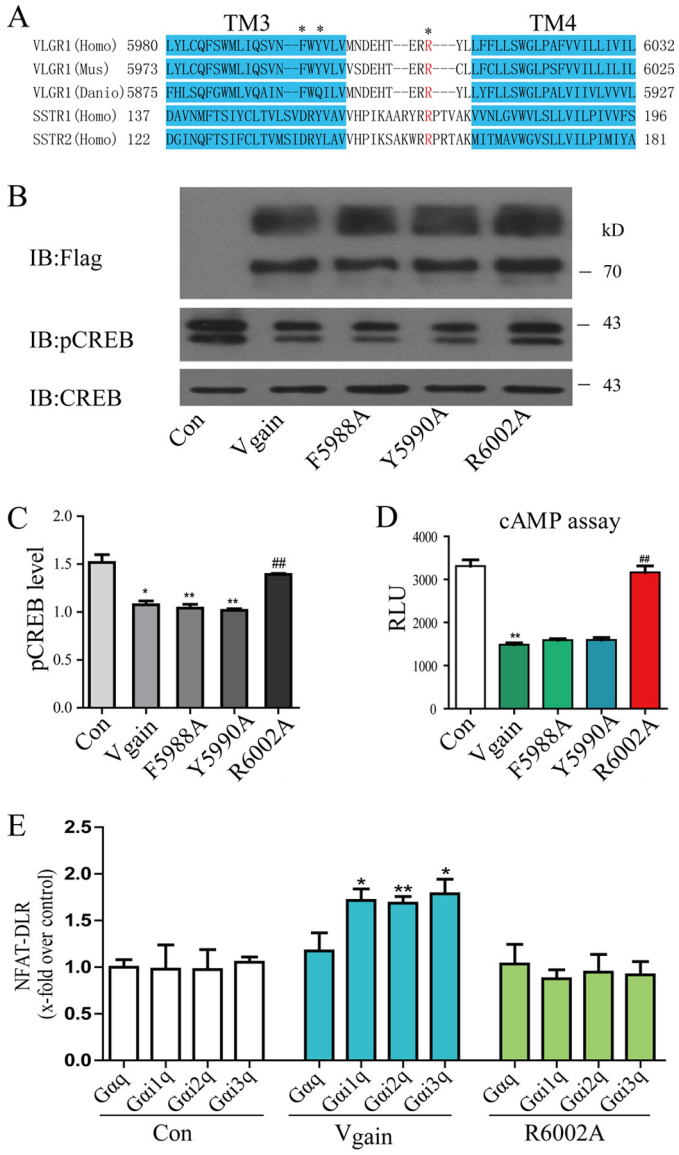

FIGURE 4. **Structural requirements for VLGR1-Gα$_i$ protein coupling.** *A*, the sequence alignments of transmembrane domains 3 (*TM3*) and 4 (*TM4*) and intracellular loop 2 of VLGR1 from different species and from the Gα$_i$-coupled receptors SSTR1 and SSTR2. Selective mutations are highlighted by *. *B*, the effects of V_{gain} and V_{gain} mutants on forskolin-induced CREB phosphorylation. The expression levels of V_{gain} and the V_{gain} mutants were detected using a FLAG-specific antibody, and CREB phosphorylation was examined using a phospho-CREB-Ser^{133}-specific antibody (*pCREB*). *C*, statistics of *B*. *, $p < 0.05$; **, $p < 0.01$ for V_{gain} wild type- or V_{gain} mutant-transfected cells compared with control vector-transfected cells; ##, $p < 0.01$ for specific V_{gain} mutant compared with V_{gain} wild type. *Error bars* represent S.D. *D*, the effects of V_{gain} and V_{gain} mutants on forskolin-induced cAMP levels. GloSensor cAMP HEK293 cells were transfected with equal amounts of V_{gain} or V_{gain} mutants. The intracellular cAMP levels were monitored with FLIPR^{TETRA}. ***, $p < 0.005$ compared with control; ###, $p < 0.005$ compared with V_{gain}-transfected cells. *Error bars* represent S.D. *E*, the plasmids encoding the Gα$_q$ or the Gα$_{iq}$ chimeric proteins were co-transfected with the control vector, V_{gain}, or V_{gain}-R6002A mutant. The activation of the Gα$_{iq}$-PLC pathway by V_{gain}-R6002A mutant was compared with V_{gain}. *, $p < 0.05$; **, $p < 0.01$ compared with control vector. *Error bars* represent S.E. *Con*, control; *IB*, immunoblot; *RLU*, relative luciferase units; *DLR*, Dual-Luciferase reporter.

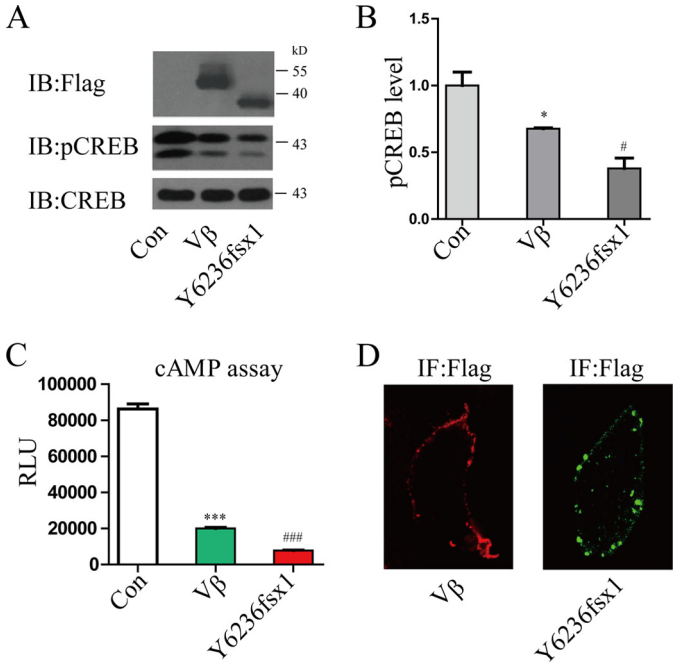

FIGURE 5. **Regulation of VLGR1-Gα$_i$ signaling by a VLGR1 pathogenic mutant.** *A*, the effects of V_β and V_β-Y6236fsx1 on forskolin-induced CREB phosphorylation. The expression levels of the receptor and phospho-CREB-Ser^{133} (*pCREB*) were detected using their specific antibodies. *B*, statistics of *A*. **, $p < 0.01$ compared with control cells; #, $p < 0.05$ compared with V_β-transfected cells. *Error bars* represent S.D. *C*, the effects of V_β and V_β-Y6236fsx1 on the forskolin-induced cAMP level examined using the GloSensor cAMP assay. ***, $p < 0.005$ compared with control; ###, $p < 0.005$ compared with V_β-transfected cells. *Error bars* represent S.D. *D*, immunofluorescence of V_β and V_β-Y6236fsx1 showed that V_β-Y6236fsx1 had unchanged receptor membrane localization. Plasmids encoding FLAG-tagged V_β or V_β-Y6236fsx1 were transiently transfected in HEK293 cells, and their cellular localization was monitored with an anti-FLAG antibody and confocal microscopy. *Con*, control; *IB*, immunoblot; *RLU*, relative luciferase units; *IF*, immunofluorescence.

increases their binding affinity to agonist and increases the basal activity of the effector in the case of some GPCRs, such as GPR120 (28–30). Our results showed that, compared with V_{gain}, V_{gi} has a stronger AC inhibitory activity, whereas the V_{gs} has a weaker activity likely due to the blockade of the interaction of V_{gain} with endogenous Gα$_i$ protein (Fig. 3*D*). Forskolin-induced CREB phosphorylation also decreased more when V_{gi} was overexpressed than when V_{gain} was overexpressed (Fig. 3, *E* and *F*).

We further used the Gα$_{iq}$ chimeric protein to examine the G protein coupling specificity of V_{gain} and V_β. It has been shown that the substitution of the last four to five C-terminal amino acids of Gα$_i$ with the corresponding residues of Gα$_q$ makes the Gα$_{iq}$ chimera couple to Gα$_i$-coupled receptors but signal through the Gα$_q$-mediated phospholipase C pathway (26, 31). We made three Gα$_{iq}$ chimeras and examined their effects on the Gα$_q$ signaling pathway in V_{gain}- and V_β-transfected cells using the pcDNA3.1 plasmid as a negative control and the dopamine D2 receptor as a positive control (Fig. 3*G*). In pcDNA3.1-transfected cells, the overexpression of the three Gα$_{iq}$ chimeras did not increase the activation of the Gα$_q$ downstream NFAT reporter gene. However, after transfection with dopamine D2 receptor, V_{gain}, or V_β, these chimeras rerouted signaling to the PLC$_\beta$-NFAT signaling pathway (Fig. 3*H*). Notably, Gα$_{i1q}$, Gα$_{i2q}$, and Gα$_{i3q}$ all increased the signaling of the PLC pathway in the presence of V_{gain} and V_β, suggesting that V_{gain} and V_β recognize all three Gα$_i$ subtypes.

Structural Requirements for the Gα$_i$ Protein Coupling of VLGR1—To further confirm that the constitutive activity of V_{gain} and V_β are specific to Gα$_i$, we next looked for potential

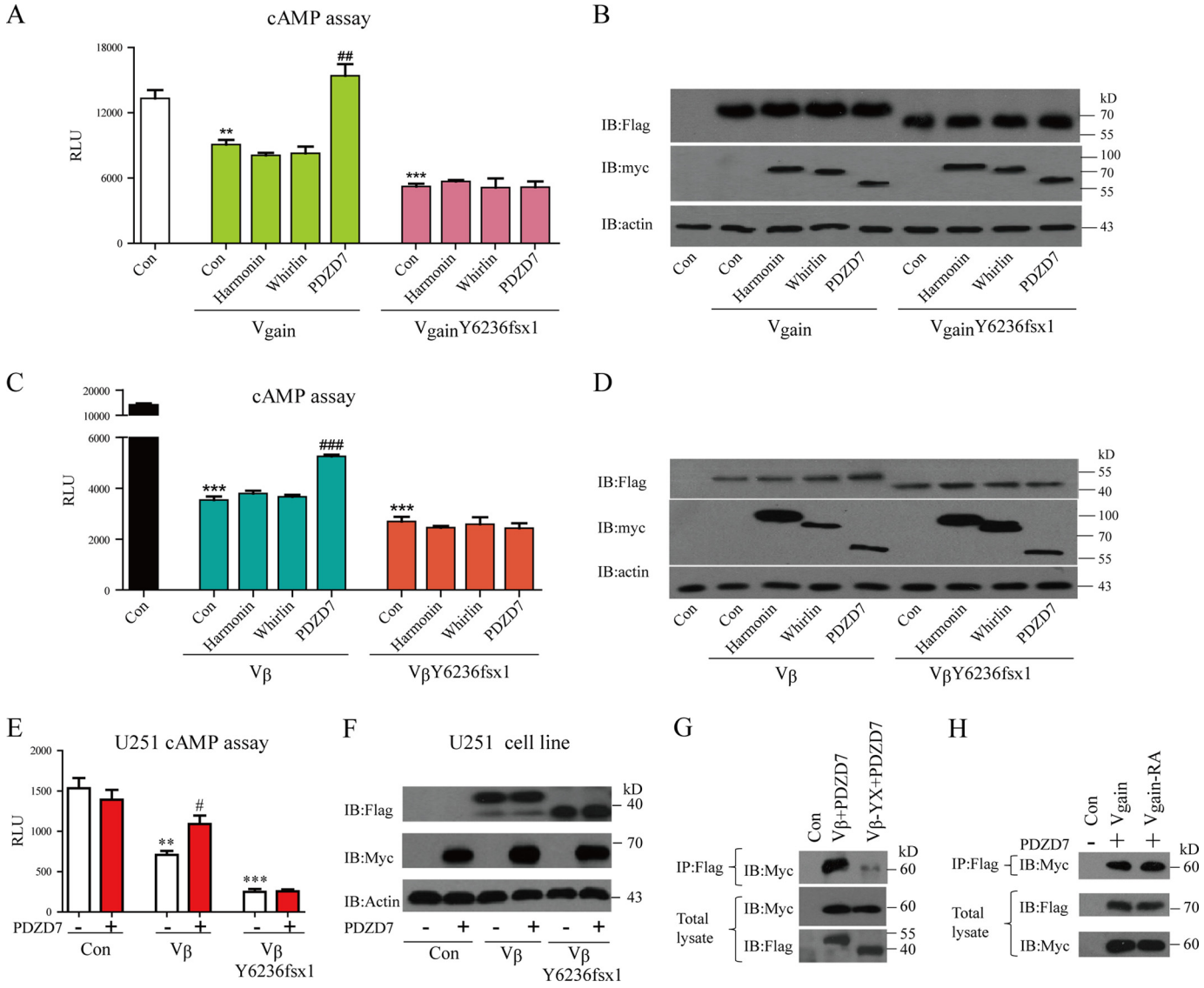

FIGURE 6. **Regulation of VLGR1-Gα$_i$ signaling by PDZD7.** *A*, effects of Usher proteins on V_{gain}-Gα$_i$ or V_{gain}-Y6236fsX1-Gα$_i$ coupling. Equal amounts of Usher proteins, including Harmonin, Whirlin, and PDZD7, were co-expressed with V_{gain} or V_{gain}-Y6236fsX1. The forskolin-induced cAMP increase were monitored by GloSensor cAMP assay. Harmonin or Whirlin has no effect on AC inhibitory activity of V_{gain} or V_{gain}-Y6236fsX1. Although PDZD7 decouples V_{gain}-Gα$_i$ interaction, it has no effect on V_{gain}-Y6236fsX1-Gα$_i$ coupling. **, $p < 0.01$, ***, $p < 0.005$ compared with control cells; ##, $p < 0.01$ compared with V_{gain} only-transfected cells. *Error bars* represent S.D. *C*, the effects of the overexpression of PDZ domain-containing Usher proteins, including Harmonin, Whirlin, and PDZD7, on the effects of $V_β$- and $V_β$-Y6236fsx1-induced AC inhibition. Equal amounts of the cDNAs encoding Harmonin, Whirlin, or PDZD7 were co-transfected with $V_β$ or $V_β$-Y6236fsx1 in GloSensor cAMP HEK293 cells. The forskolin-induced cAMP levels were examined. ***, $p < 0.005$ compared with control cells; ###, $p < 0.005$ compared with $V_β$ only-transfected cells. *Error bars* represent S.D. *B* and *D*, expression of FLAG-tagged V_{gain} (*A*) and $V_β$ (*C*). Myc-tagged Harmonin, Whirlin, and PDZD7 in *B* and *D* were detected with specific anti-FLAG and anti-Myc antibodies. *E*, the effects of the overexpression of the PDZD7 on the effects of $V_β$- and $V_β$-Y6236fsx1-induced AC inhibition. The PDZD7 and GloSensor plasmids were co-transfected with $V_β$ or $V_β$-Y6236fsx1 in U251 cells. The forskolin-induced cAMP levels were examined. **, $p < 0.01$; ***, $p < 0.005$ compared with control cells; #, $p < 0.05$ compared with $V_β$ only-transfected cells. *Error bars* represent S.D. *F*, expression of FLAG-tagged $V_β$ and Myc-tagged PDZD7 in *E* was detected with specific anti-FLAG and anti-Myc antibodies. *G*, FLAG-tagged $V_β$ or $V_β$-Y6236fsx1 was co-transfected with Myc-tagged PDZD7 in HEK293 cells. The VLGR1·PDZD7 complex was immunoprecipitated with an anti-FLAG antibody and detected with an anti-Myc antibody. *H*, formation of the V_{gain}·PDZD7 or V_{gain}-R6002A·PDZD7 complex was detected as in *G*. *Con*, control; *IB*, immunoblot; *RLU*, relative luciferase units.

mutations that would specifically decouple the interaction between VLGR1 and Gα$_i$. In the recently solved $β_2$-adrenergic receptor·Gα$_s$ complex crystal structure, intracellular loop 2 of the $β_2$-adrenergic receptor forms extensive interactions with the N terminus of Gα$_s$. In particular, Phe^{139} of $β_2$-adrenergic receptor intracellular loop 2 is inserted into the hydrophobic pocket formed by His^{41}, Val^{217}, Phe^{376}, and Arg^{380} of Gα$_s$ (32). This hydrophobic interaction may be a driving force for $β_2$-adrenergic receptor and Gα$_s$ coupling. Assuming that the residues around intracellular loop 2 of VLGR1 are also important for G protein coupling, we examined the effects of mutating several conserved residues of VLGR1 (Fig. 4, *A*, *B*, and *C*). All of the mutants had normal expression levels and did not affect the cell surface localization of the receptor. The Phe^{5988} and Tyr^{5990} mutations did not significantly affect the inhibitory activity of V_{gain}, but the R6002A mutation eliminated the inhibition of V_{gain} toward the forskolin-induced cAMP increase (Fig. 4, *B*, *C*, and *D*). The R6002A mutant may directly impair Gα$_i$ protein coupling ability as demonstrated by the Gα$_{iq}$ chimera switching assay (Fig. 4*E*). Although overexpression of Gα$_{i1q}$, Gα$_{i2q}$, or

$G\alpha_{i3q}$ promoted PLC signaling in the presence of the wild type V_{gain}, they produced no effects in the presence of the R6002A V_{gain} mutant. These results verified that the AC inhibitory activity was directly linked to the intact seven-transmembrane structure of VLGR1.

A Disease-associated Mutant Has a Gain of Function in $G\alpha_i$ Coupling—Among the disease-associated VLGR1 mutations, the VLGR1 human Y6244fsX1 caught our attention because it is located in the intracellular part of the receptor (3). We therefore made a mouse VLGR1 Y6236fsx1 mutant that corresponds with the human Y6244fsx1 cDNA. Notably, the pathogenic Y6236fsx1 mutation has a frameshift that eliminates the last 62 residues of the C terminus, producing a 39-kDa band after gel electrophoresis (Fig. 5*A*). The Y6236fsx1 mutation did not change the plasma membrane receptor localization detected by immunofluorescence (Fig. 5*D*). However, the introduction of the Y6236fsx1 mutation into V_β or V_{gain} increased their inhibitory effects on AC activity as demonstrated by the GloSensor assay and phospho-CREB levels (Figs. 5, *B* and *C*, and 6, *A*–*D*). These results suggest that the pathogenic mutation Y6236fsx1 increases its $G\alpha_i$ coupling ability.

PDZD7 Negatively Regulated $G\alpha_i$ Coupling Activity in V_{gain} and V_β—Because of its short C-terminal tail, the pathogenic VLGR1 Y6236fsx1 mutation may affect its binding to downstream effectors and contribute to its increased $G\alpha_i$ coupling activity. We thus overexpressed three known VLGR1 C terminus-interacting partners, Harmonin, Whirlin, and PDZD7, all of which are involved in Usher syndrome, to investigate their effects on VLGR1-mediated AC inhibition (33, 34). Interestingly, although overexpression of Harmonin or Whirlin had no effect on VLGR1-mediated AC inhibition, overexpression of the other Usher syndrome-related protein, PDZD7, inhibited both V_{gain}- and V_β-mediated AC inhibition (Fig. 6, *A*–*D*). However, the overexpression of PDZD7 did not block Y6236fx1-mediated AC inhibition (Fig. 6, *A*–*D*). The specific inhibition of V_β but not V_β-Y6236fx1 activity by PDZD7 was also demonstrated in the neuronal glioblastoma (astrocytoma) cell line U251 (Fig. 6, *E* and *F*).

Removing the C-terminal PDZ binding motif "DTHL" has been shown to significantly reduce the interaction between PDZD7 and the VLGR1 C-tail (1, 12). The effects of a loss of PDZD7 on Y6236fx1 mutants may be due to the loss of the interaction between these two proteins. Consistent with this hypothesis, the V_β-Y6236fx1 mutation significantly reduced its interaction with PDZD7 compared with V_β (Fig. 6*G*). In contrast, both the V_{gain}- and V_{gain}-R6002A mutants robustly co-immunoprecipitated with PDZD7 in equal amounts (Fig. 6*H*). These results suggested that the Y6236fsx1 mutation improved VLGR1 inhibitory activity on AC likely due to the loss of interaction with its C-terminal binding partners, such as PDZD7. However, the loss of function in the R6002A mutant did not alter its interaction with PDZD7. Whether the gain of function in $G\alpha_i$ signaling by the VLGR1 Y6236sfx1 mutant contributes to the development of Usher syndrome awaits further investigation.

Conclusion—In summary, we have demonstrated that the Usher protein VLGR1 can be separated into two subunits by autocleavage at its GPS. Without extracellular stimulation, the β-subunit of VLGR1 inhibits AC activity through $G\alpha_i$ coupling. Its $G\alpha_i$ coupling specificity was verified using site-directed mutagenesis, PTX interference, and receptor-G protein fusion proteins as well as co-expression with the $G\alpha_{iq}$ chimeric protein. Moreover, the intracellular pathogenic mutation VLGR1 Y6236fsx1 had an increased constitutive activation of $G\alpha_i$ signaling. The overexpression of the Usher protein PDZD7 blocked VLGR1 β-subunit-mediated AC inhibition, but PDZD7 had no effect on Y6236fsx1 mutant-mediated AC inhibition. Recent studies have identified the digenic inheritance of PDZD7 and VLGR1 as well as the physical interaction between PDZD7 and the VLGR1 C terminus. However, the molecular mechanism underlying this genetic linkage is unclear (12, 35). The association of the Usher protein PDZD7 as well as the Usher mutant VLGR1 Y6236fsx1 with $G\alpha_i$ activity suggests a potential role for VLGR1-mediated $G\alpha_i$ signaling in Usher disease development.

Recently, a parallel work showed that a recombinant VLGR1 truncation protein senses extracellular calcium, activates $G\alpha_s$ and $G\alpha_q$ signaling, and regulates the stability of myelin-associated glycoprotein, which is important for the prevention of audiogenic epilepsy (14). Although the reported G protein subtype signaling downstream of VLGR1 is different from that in our study, the known beneficial effects of AC activation in the prevention of audiogenic epilepsy are logically consistent with our finding that the disease-associated VLGR1 mutant inhibited AC activity (14). Moreover, the switching of G protein coupling specificity in different physiological/pathological conditions has been demonstrated in other GPCRs, such as the β_2-adrenergic receptor in which the receptor phosphorylation by PKA switched its coupling from $G\alpha_s$ to $G\alpha_i$ (36, 37). Our result showed that V_β has stronger $G\alpha_i$ coupling activity than V_{gain}, suggesting that the N-terminal fragment has an inhibitory role in VLGR1 activity. Thus, it is likely that the cleaved V_β subunit signals independently and switched the VLGR1 G protein coupling specificity. Taken together, our data show the constitutive $G\alpha_i$ coupling activity of the VLGR1 β-subunit and the regulation of this activity by the N terminus of VLGR1, a disease-associated mutant, and the Usher protein PDZD7. This study may shed light on the molecular mechanisms underlying Usher syndrome.

REFERENCES

1. Sun, J. P., Li, R., Ren, H. Z., Xu, A. T., Yu, X., and Xu, Z. G. (2013) The very large G protein coupled receptor (Vlgr1) in hair cells. *J. Mol. Neurosci.* **50,** 204–214
2. McMillan, D. R., and White, P. C. (2010) Studies on the very large G protein-coupled receptor: from initial discovery to determining its role in sensorineural deafness in higher animals. *Adv. Exp. Med. Biol.* **706,** 76–86
3. Weston, M. D., Luijendijk, M. W., Humphrey, K. D., Möller, C., and Kimberling, W. J. (2004) Mutations in the VLGR1 gene implicate G-protein signaling in the pathogenesis of Usher syndrome type II. *Am. J. Hum. Genet.* **74,** 357–366
4. Nakayama, J., Fu, Y. H., Clark, A. M., Nakahara, S., Hamano, K., Iwasaki, N., Matsui, A., Arinami, T., and Ptácek, L. J. (2002) A nonsense mutation of the MASS1 gene in a family with febrile and afebrile seizures. *Ann. Neurol.* **52,** 654–657
5. McGee, J., Goodyear, R. J., McMillan, D. R., Stauffer, E. A., Holt, J. R., Locke, K. G., Birch, D. G., Legan, P. K., White, P. C., Walsh, E. J., and Richardson, G. P. (2006) The very large G-protein-coupled receptor VLGR1: a component of the ankle link complex required for the normal

development of auditory hair bundles. *J. Neurosci.* **26,** 6543–6553
6. Michalski, N., Michel, V., Bahloul, A., Lefèvre, G., Barral, J., Yagi, H., Chardenoux, S., Weil, D., Martin, P., Hardelin, J. P., Sato, M., and Petit, C. (2007) Molecular characterization of the ankle-link complex in cochlear hair cells and its role in the hair bundle functioning. *J. Neurosci.* **27,** 6478–6488
7. Maerker, T., van Wijk, E., Overlack, N., Kersten, F. F., McGee, J., Goldmann, T., Sehn, E., Roepman, R., Walsh, E. J., Kremer, H., and Wolfrum, U. (2008) A novel Usher protein network at the periciliary reloading point between molecular transport machineries in vertebrate photoreceptor cells. *Hum. Mol. Genet.* **17,** 71–86
8. Yang, J., Liu, X., Zhao, Y., Adamian, M., Pawlyk, B., Sun, X., McMillan, D. R., Liberman, M. C., and Li, T. (2010) Ablation of whirlin long isoform disrupts the USH2 protein complex and causes vision and hearing loss. *PLoS Genet.* **6,** e1000955
9. Paavola, K. J., and Hall, R. A. (2012) Adhesion G protein-coupled receptors: signaling, pharmacology, and mechanisms of activation. *Mol. Pharmacol.* **82,** 777–783
10. van Wijk, E., van der Zwaag, B., Peters, T., Zimmermann, U., Te Brinke, H., Kersten, F. F., Märker, T., Aller, E., Hoefsloot, L. H., Cremers, C. W., Cremers, F. P., Wolfrum, U., Knipper, M., Roepman, R., and Kremer, H. (2006) The DFNB31 gene product whirlin connects to the Usher protein network in the cochlea and retina by direct association with USH2A and VLGR1. *Hum. Mol. Genet.* **15,** 751–765
11. Reiners, J., van Wijk, E., Märker, T., Zimmermann, U., Jürgens, K., te Brinke, H., Overlack, N., Roepman, R., Knipper, M., Kremer, H., and Wolfrum, U. (2005) Scaffold protein harmonin (USH1C) provides molecular links between Usher syndrome type 1 and type 2. *Hum. Mol. Genet.* **14,** 3933–3943
12. Ebermann, I., Phillips, J. B., Liebau, M. C., Koenekoop, R. K., Schermer, B., Lopez, I., Schäfer, E., Roux, A. F., Dafinger, C., Bernd, A., Zrenner, E., Claustres, M., Blanco, B., Nürnberg, G., Nürnberg, P., Ruland, R., Westerfield, M., Benzing, T., and Bolz, H. J. (2010) PDZD7 is a modifier of retinal disease and a contributor to digenic Usher syndrome. *J. Clin. Investig.* **120,** 1812–1823
13. Paavola, K. J., Stephenson, J. R., Ritter, S. L., Alter, S. P., and Hall, R. A. (2011) The N terminus of the adhesion G protein-coupled receptor GPR56 controls receptor signaling activity. *J. Biol. Chem.* **286,** 28914–28921
14. Shin, D., Lin, S. T., Fu, Y. H., and Ptácek, L. J. (2013) Very large G protein-coupled receptor 1 regulates myelin-associated glycoprotein via Gαs/Gαq-mediated protein kinases A/C. *Proc. Natl. Acad. Sci. U.S.A.* **110,** 19101–19106
15. Xu, Z., Peng, A. W., Oshima, K., and Heller, S. (2008) MAGI-1, a candidate stereociliary scaffolding protein, associates with the tip-link component cadherin 23. *J. Neurosci.* **28,** 11269–11276
16. de Melo, J., and Blackshaw, S. (2011) *In vivo* electroporation of developing mouse retina. *J. Vis. Exp.* **52,** e2847
17. Luttrell, L. M., Ferguson, S. S., Daaka, Y., Miller, W. E., Maudsley, S., Della Rocca, G. J., Lin, F., Kawakatsu, H., Owada, K., Luttrell, D. K., Caron, M. G., and Lefkowitz, R. J. (1999) β-Arrestin-dependent formation of β2 adrenergic receptor-Src protein kinase complexes. *Science* **283,** 655–661
18. Araç, D., Boucard, A. A., Bolliger, M. F., Nguyen, J., Soltis, S. M., Südhof, T. C., and Brunger, A. T. (2012) A novel evolutionarily conserved domain of cell-adhesion GPCRs mediates autoproteolysis. *EMBO J.* **31,** 1364–1378
19. Lin, H. H., Chang, G. W., Davies, J. Q., Stacey, M., Harris, J., and Gordon, S. (2004) Autocatalytic cleavage of the EMR2 receptor occurs at a conserved G protein-coupled receptor proteolytic site motif. *J. Biol. Chem.* **279,** 31823–31832
20. McMillan, D. R., Kayes-Wandover, K. M., Richardson, J. A., and White, P. C. (2002) Very large G protein-coupled receptor-1, the largest known cell surface protein, is highly expressed in the developing central nervous system. *J. Biol. Chem.* **277,** 785–792
21. Nikkila, H., McMillan, D. R., Nunez, B. S., Pascoe, L., Curnow, K. M., and White, P. C. (2000) Sequence similarities between a novel putative G protein-coupled receptor and Na^+/Ca^{2+} exchangers define a cation binding domain. *Mol. Endocrinol.* **14,** 1351–1364
22. Skradski, S. L., Clark, A. M., Jiang, H., White, H. S., Fu, Y. H., and Ptácek, L. J. (2001) A novel gene causing a mendelian audiogenic mouse epilepsy. *Neuron* **31,** 537–544
23. Bonnet, C., and El-Amraoui, A. (2012) Usher syndrome (sensorineural deafness and retinitis pigmentosa): pathogenesis, molecular diagnosis and therapeutic approaches. *Curr. Opin. Neurol.* **25,** 42–49
24. Stephenson, J. R., Paavola, K. J., Schaefer, S. A., Kaur, B., Van Meir, E. G., and Hall, R. A. (2013) Brain-specific angiogenesis inhibitor-1 signaling, regulation, and enrichment in the postsynaptic density. *J. Biol. Chem.* **288,** 22248–22256
25. Ward, Y., Lake, R., Yin, J. J., Heger, C. D., Raffeld, M., Goldsmith, P. K., Merino, M., and Kelly, K. (2011) LPA receptor heterodimerizes with CD97 to amplify LPA-initiated RHO-dependent signaling and invasion in prostate cancer cells. *Cancer Res.* **71,** 7301–7311
26. Bohnekamp, J., and Schöneberg, T. (2011) Cell adhesion receptor GPR133 couples to Gs protein. *J. Biol. Chem.* **286,** 41912–41916
27. Hase, M., Yokomizo, T., Shimizu, T., and Nakamura, M. (2008) Characterization of an orphan G protein-coupled receptor, GPR20, that constitutively activates G_i proteins. *J. Biol. Chem.* **283,** 12747–12755
28. Hirasawa, A., Tsumaya, K., Awaji, T., Katsuma, S., Adachi, T., Yamada, M., Sugimoto, Y., Miyazaki, S., and Tsujimoto, G. (2005) Free fatty acids regulate gut incretin glucagon-like peptide-1 secretion through GPR120. *Nat. Med.* **11,** 90–94
29. Holliday, N. D., Watson, S. J., and Brown, A. J. (2011) Drug discovery opportunities and challenges at G protein coupled receptors for long chain free fatty acids. *Front. Endocrinol.* **2,** 112
30. Bertin, B., Freissmuth, M., Jockers, R., Strosberg, A. D., and Marullo, S. (1994) Cellular signaling by an agonist-activated receptor/Gsα fusion protein. *Proc. Natl. Acad. Sci. U.S.A.* **91,** 8827–8831
31. Conklin, B. R., Farfel, Z., Lustig, K. D., Julius, D., and Bourne, H. R. (1993) Substitution of three amino acids switches receptor specificity of Gqα to that of Giα. *Nature* **363,** 274–276
32. Rasmussen, S. G., DeVree, B. T., Zou, Y., Kruse, A. C., Chung, K. Y., Kobilka, T. S., Thian, F. S., Chae, P. S., Pardon, E., Calinski, D., Mathiesen, J. M., Shah, S. T., Lyons, J. A., Caffrey, M., Gellman, S. H., Steyaert, J., Skiniotis, G., Weis, W. I., Sunahara, R. K., and Kobilka, B. K. (2011) Crystal structure of the β2 adrenergic receptor-Gs protein complex. *Nature* **477,** 549–555
33. Zallocchi, M., Meehan, D. T., Delimont, D., Rutledge, J., Gratton, M. A., Flannery, J., and Cosgrove, D. (2012) Role for a novel Usher protein complex in hair cell synaptic maturation. *PLoS One* **7,** e30573
34. Zallocchi, M., Delimont, D., Meehan, D. T., and Cosgrove, D. (2012) Regulated vesicular trafficking of specific PCDH15 and VLGR1 variants in auditory hair cells. *J. Neurosci.* **32,** 13841–13859
35. Zou, J., Zheng, T., Ren, C., Askew, C., Liu, X. P., Pan, B., Holt, J. R., Wang, Y., and Yang, J. (2014) Deletion of PDZD7 disrupts the Usher syndrome type 2 protein complex in cochlear hair cells and causes hearing loss in mice. *Hum. Mol. Genet.* **23,** 2374–2390
36. Daaka, Y., Luttrell, L. M., and Lefkowitz, R. J. (1997) Switching of the coupling of the β2-adrenergic receptor to different G proteins by protein kinase A. *Nature* **390,** 88–91
37. Xiao, R. P., Zhang, S. J., Chakir, K., Avdonin, P., Zhu, W., Bond, R. A., Balke, C. W., Lakatta, E. G., and Cheng, H. (2003) Enhanced G_i signaling selectively negates β2-adrenergic receptor (AR)–but not β1-AR-mediated positive inotropic effect in myocytes from failing rat hearts. *Circulation* **108,** 1633–1639